Journal of Zhejiang University-SCIENCE B (Biomedicine & Biotechnology) *2022 23(4):328-338*
www.jzus.zju.edu.cn; www.springer.com/journal/11585
E-mail: jzus_b@zju.edu.cn

Research Article

https://doi.org/10.1631/jzus.B2100682

Shoot rot of *Zizania latifolia* and the first record of its pathogen *Pantoea ananatis* in China

Zilan XIAO[1], Jianping DENG[2], Xiaojun ZHOU[3], Liyan ZHU[3], Xiaochan HE[3], Jingwu ZHENG[1], Deping GUO[4]✉, Jingze ZHANG[1]✉

[1]*Ministry of Agriculture Key Lab of Molecular Biology of Crop Pathogens and Insects, Institute of Biotechnology, Zhejiang University, Hangzhou 310058, China*
[2]*Plant Protection and Plant Inspection Station of Jinyun County, Jinyun 321401, China*
[3]*Jinhua Academy of Agricultural Sciences, Jinhua 321017, China*
[4]*Department of Horticulture, College of Agriculture and Biotechnology, Zhejiang University, Hangzhou 310058, China*

Abstract: The aquatic grass *Zizania latifolia* grows symbiotically with the fungus *Ustilago esculenta* producing swollen structures called Jiaobai, widely cultivated in China. A new disease of *Z. latifolia* was found in Zhejiang Province, China. Initial lesions appeared on the leaf sheaths or sometimes on the leaves near the leaf sheaths. The lesions extended along the axis of the leaf shoots and formed long brown to dark brown streaks from the leaf sheath to the leaf, causing sheath rot and death of entire leaves on young plants. The pathogen was isolated and identified as the bacterium *Pantoea ananatis*, based on 16S ribosomal RNA (rRNA) gene sequencing, multilocus sequence analysis (*atpD* (β-subunit of ATP synthase F1), *gyrB* (DNA gyrase subunit B), *infB* (translation initiation factor 2), and *rpoB* (β-subunit of RNA polymerase) genes), and pathogenicity tests. Ultrastructural observations using scanning electron microscopy revealed that the bacterial cells colonized the vascular tissues in leaf sheaths, forming biofilms on the inner surface of vessel walls, and extended between vessel elements via the perforated plates. To achieve efficient detection and diagnosis of *P. ananatis*, species-specific primer pairs were designed and validated by testing closely related and unrelated species and diseased tissues of *Z. latifolia*. This is the first report of bacterial sheath rot disease of *Z. latifolia* caused by *P. ananatis* in China.

Key words: *Zizania latifolia*; Phylogeny; *Pantoea ananatis*; Multilocus analysis; Scanning electron microscopy; Species-specific primers

1 Introduction

Zizania latifolia (Griseb.) Turcz. ex Stapf, belongs to the rice tribe (Oryzeae, Poaceae) (Xu et al., 2009) and grows symbiotically with a smut fungus, *Ustilago esculenta* Henn., causing swelling of its upper culms. The swollen culms have traditionally been used as an aquatic vegetable, commonly called Jiaobai in China (Zhang et al., 2012). Due to its unique flavor and delicacy, Jiaobai has been cultivated in China for more than 2000 years (Zhang et al., 2012, 2014). In recent years, the Jiaobai cultivation area has steadily increased with China's rapid economic development, but disease is becoming more severe in some regions. The major diseases of Jiaobai plants are brown spot and rust, which occur in almost all cultivation areas in China. Brown spot is one of the most severe leaf spot diseases of this crop. It is caused by *Bipolaria oryzae* (Xiao et al., 2015). This pathogen was first described as *Helminthosporium zizaniae* by Nisikado (1929), but was later identified as *Bipolaris zizaniae* (Shoemaker, 2006). However, based on morphological characteristics, molecular data, and phylogenetic studies, *B. zizaniae* is considered conspecific with *B. oryzae* (Xiao et al., 2015). *B. oryzae* is regarded as the correct name according to priorities regulation. Serious outbreaks of Jiaobai rust, caused by *Uromyces coronatus* Miyabe et Nishida ex Dietel, usually occur each year, especially in mountainous areas (Deng et al.,

✉ Jingze ZHANG, jzzhang@zju.edu.cn
Deping GUO, dpguo@zju.edu.cn
Jingze ZHANG, https://orcid.org/0000-0001-8604-8280
Deping GUO, https://orcid.org/0000-0002-1266-8353

Received Aug. 2, 2021; Revision accepted Nov. 3, 2021;
Crosschecked Mar. 23, 2022

2015). Brown spot and rust generally occur at different growth stages, leading to whole or partial leaf wilt on a plant before the end of the growing season. In addition, a basal stalk rot of Jiaobai plants has been reported in Taiwan, China, caused by *Pythiogeton zizaniae* (Ann et al., 2006). Infection by *P. zizaniae* causes yellowing and browning of young leaves of Jiaobai, and basal stem rot. Eventually, infected plants die (Ann et al., 2006). However, in June 2019, an unusual disease of Jiaobai plants was found in Jinyun County of Lishui City, Zhejiang Province, China. In this study, we identified the pathogen, conducted pathogenicity tests, observed pathogen colonization and extension characteristics in diseased tissue, and designed specific primer pairs to detect the pathogen. These results will provide critical information for controlling this new disease and preventing its dispersal.

2 Materials and methods

2.1 Observation of the symptoms and pathogen isolation

Disease symptoms were observed throughout the growing season in Dayang Town, Jinyun County, Lishui City, Zhejiang Province, China in 2019. Diseased samples were collected from *Z. latifolia* cv. Mayrenjiao from five different sites early in June 2019. For each sample, a piece of diseased tissue (about 3 mm×5 mm) was excised from the margin of a lesion between healthy and diseased zones on a leaf sheath. The samples were surface-sterilized for 2 min in 75% (volume fraction) ethanol, followed by rinsing in sterile distilled water three times. Pieces of each sample were placed in a sterilized mortar and mashed with a pestle after adding 2 mL sterile water. Next, to exclude saprophytic microbes, 100 μL of tissue sap was injected into the leaf sheaths of seedlings cultivated in pots. For symptom observations, the pots were incubated under a light-dark cycle (light: 16 h, 28 ℃; dark: 8 h, 25 ℃). Diseased spots were excised once larger than 0.5 cm, and sap was obtained from the diseased tissue as described above. After the sap obtained was inoculated again, the tissue sap obtained with the same method was streaked onto lysogeny broth (LB) agar (yeast extract 5 g, tryptone 10 g, NaCl 10 g, agar 15 g, pH 7.2–7.5), and plates were incubated at 30 ℃ for 20–24 h. Different colonies were chosen based on characteristics such as their shape (regular or irregular, convex or flat), color, and size. Subsequently, each colony was purified at least three times, and then used for pathogenicity tests.

2.2 Pathogenicity tests

Triplet cuttings of *Z. latifolia* cv. Mayrenjiao with 3–5 nodes from a disease-free field at the end of harvest were cultivated in plastic pots containing sterilized rice field soil. The pots were placed in a greenhouse with a relative humidity of 70%–80% and temperature of 25–30 ℃. After growing on for two months, the plants were used for inoculation. Cell suspensions of the test strains were prepared in LB on a rotary shaker for 150 r/min at 30 ℃ for 24 h. The bacterial cells were harvested by centrifugation, washed, and resuspended in sterile physiological saline. An inoculum containing about 1×10^8 colony-forming units (CFU)/mL was prepared for each test strain. A volume of 100 μL cell suspension was injected into the leaf sheaths. Each treatment for each strain was repeated four times, and sterile water-injection treatments were used as a control. The inoculated leaf sheaths were wrapped in plastic film for 48 h, and kept under the same conditions as described above. Symptoms of disease were observed daily. The pathogenic strains were re-isolated, purified, and compared with the inoculated strains based on their colony characteristics. Representative strains were selected based on the sample origin and deposited at −70 ℃ in 25% (volume fraction) glycerol in the Culture Collection of Biotechnology Institute, Zhejiang University, Hangzhou, China.

2.3 Identification of bacterial strains

Representative strains from different sites were selected for molecular identification. The colonies were grown on LB agar at 30 ℃ for 18–24 h and characterized as described by Zhang et al. (2018). The 16S ribosomal RNA (rRNA) gene was amplified by polymerase chain reaction (PCR) for each representative bacterial strain in an automated thermal cycler (Eppendorf AG, Germany) with universal primers: 27F (5'-AGAGTTTGATCATGGCTCAG-3') as forward primer and 1492R (5'-GGTTACCTTGTTACGACTT-3') as reverse primer (Lane et al., 1985; Lane, 1991; Turner et al., 1999). The amplified products were checked on a 1% (0.01 g/mL) agarose gel under an

ultraviolet transilluminator, and then sent to the Qingke Biotech Co., Ltd. (Hangzhou, China) for sequencing both strands. The resulting sequence was analyzed and compared with others in the GenBank database using the BLAST search tool, after they were edited using Bioedit Version 7.19 (Hall, 1999). Phylogenetic trees were generated using the neighbor-joining method with the molecular evolutionary genetics analysis (MEGA) program (Version 7.0) (Kumar et al., 2016). Bootstrap replication (1000) was used as statistical analysis for the nodes in the phylogenetic trees.

For multilocus sequence analysis (MLSA), four housekeeping genes, *gyrB* (DNA gyrase subunit B), *rpoB* (β-subunit of RNA polymerase), *infB* (translation initiation factor 2), and *atpD* (β-subunit of ATP synthase F1), were amplified with primer pairs (Brady et al., 2008). The amplification was performed in a 50-μL reaction volume containing 5 μL 10× PCR buffer, 2 μL of each primer (20 μmol/L), 2 μL template DNA (2 μg/μL), and 0.5 μL Taq DNA polymerase (5 U/μL) (TaKaRa Bio Inc., Japan). The thermal cycling program was performed for 30 cycles after an initial denaturation at 95 ℃ for 4 min. Each cycle included a denaturation step at 95 ℃ for 1 min, annealing at a suitable temperature for 1 min, and an extension step at 72 ℃ for 1.5 min. Annealing temperatures for each reaction were 52 ℃ for *gyrB* and *rpoB*, and 50 ℃ for *atpD* and *infB* (Brady et al., 2008). The amplified products were confirmed and sequenced as described above. The resulting sequence was analyzed and submitted to the GenBank database (Table S1).

A molecular phylogenetic tree was generated by maximum likelihood (ML) using the MLSA. The sequence of each gene (*gyrB*, *rpoB*, *infB*, and *atpD*) was aligned with a multiple alignment using fast Fourier transform (MAFFT, Version 7.273) (Katoh and Standley, 2013), and the resulting sequences were analyzed by Gblocks (Version 0.91b) to eliminate ambiguously aligned positions and divergent regions before the phylogenetic analyses (Talavera and Castresana, 2007). The evolution model applied to each alignment was estimated using jModel Test (Version 2.1.7) (Darriba et al., 2012), and the model was chosen according to the Akaike information criterion. The best TIM2+I+G was selected for *gyrB*, TrNef+I+G for *rpoB*, TIM2+I+G for *infB*, and TIM2+I+G for *atpD*. ML analyses were conducted using RaxmlGUI (https://antonellilab.github.io/raxmlGUI) (Silvestro and Michalak, 2012) after the four gene sequences were concatenated by SequenceMatrix (Version 1.7.9) (Vaidya et al., 2011). ML bootstrap (ML-BS) analysis for each ML tree was performed with 1000 fast bootstrap replicates.

2.4 Scanning electron microscopy

Three pieces, each about 5 mm×5 mm, were cut from the margins of the lesions along the axis of the leaf sheaths of inoculated plants to observe pathogen colonization in infected leaf sheath tissues. They were fixed in glutaraldehyde (2.5%, volume fraction) for 48 h at 4 ℃. The samples were post-fixed in osmium tetroxide and dehydrated in a graded ethanol series followed by a few changes of isoamyl acetate for 30 min, as described by Li et al. (2017). Before critical-point drying, the samples were cut in half longitudinally. The reverse side of a cut section was mounted onto an aluminum stub with double-sided sticky film, sputter-coated with gold, and examined and photographed under a scanning electron microscope (SU8010, HITACHI, Japan).

2.5 PCR-specific primer design and pathogen detection

The PCR method was used to rapidly detect the pathogen causing disease in the fields. Species-specific primers were designed using complete gene sequences related to the bacterial classification, such as *atpD*, *gyrB*, *gltB*, *lepA*, *phaC*, *rpoB*, *infB*, *recA*, and *trpB* from *Pantoea ananatis* LMG 2665 (type strain). The nucleotide sequences were analyzed in the GenBank database at the National Center Biotechnology Information (NCBI), and genes with more significant differences were used as candidates. Genomic DNA from the five *P. ananatis* strains was amplified as previously described, except for the annealing temperature of 57 ℃, to test the specificity of the primers. The amplified products were checked on a 1% agarose gel under an ultraviolet transilluminator and photographed.

Similarly, PCR amplification of 11 strains of *Pantoea* and other genera (*Pseudomonas*, *Paenibacillus*, and *Bacillus*) was carried out using the same species-specific primers. Furthermore, samples of disease lesions and healthy leaf sheaths of Jiaobai plants were collected from different sites in Zhejiang Province (Table 1). They were cut into approximately 1-cm^2 slices, and 300 mg of each sample was frozen in liquid nitrogen and ground to powder using a mortar and

Table 1 Samples used for PCR amplification in this study

Sample*	Collection location	Latitude and longitude	Elevation (m)
ZL01 (DT)	Jinyun County, Lishui City	28°48′3″ N, 120°15′48″ E	200
ZL02 (DT)	Jinyun County, Lishui City	28°29′45″ N, 120°15′35″ E	890
ZL03 (DT)	Jinyun County, Lishui City	28°31′9″ N, 120°14′44″ E	820
ZL04 (DT)	Jinyun County, Lishui City	28°47′43″ N, 120°15′43″ E	210
ZL05 (DT)	Jinyun County, Lishui City	28°46′17″ N, 120°15′35″ E	220
ZL06 (DT)	Jinyun County, Lishui City	28°45′13″ N, 120°16′45″ E	350
ZL07 (DT)	Jinyun County, Lishui City	28°42′33″ N, 120°0′41″ E	160
ZL08 (DT)	Jinyun County, Lishui City	28°43′45″ N, 120°1′27″ E	150
ZL09 (HT)	Jinyun County, Lishui City	28°47′43″ N, 120°15′32″ E	210
ZL10 (DT)	Yuhang District, Hangzhou City	30°41′17″ N, 120°29′36″ E	12
ZL11 (DT)	Yuhang District, Hangzhou City	30°41′17″ N, 120°29′36″ E	12
ZL12 (DT)	Yuhang District, Hangzhou City	30°18′3″ N, 120°5′12″ E	10
ZL13 (HT)	Yuhang District, Hangzhou City	30°18′3″ N, 120°5′12″ E	10

* From *Zizania latifolia* in different fields. PCR: polymerase chain reaction; DT: diseased tissue; HT: healthy tissue.

pestle. Finally, the DNA extraction protocol was carried out according to the manufacturers' instructions for the Ezup Spin Column Super Plant Genomic DNA Extraction Kit (Sangon Biotech, Shanghai, China). The genomic DNA was dissolved in TE buffer (1 mmol/L Tris-HCl and 0.1 mmol/L ethylene diamine tetraacetic acid (EDTA), pH 8.0), and PCR amplification was performed as described above.

3 Results

3.1 Disease symptoms

Disease symptoms appeared from late in May to early in June, depending on the cultivation area. The disease occurred in late May in the outskirts of Hangzhou City, which is in the plain region, while in the mountainous Dayang Township, the disease appeared early in June. The initial spots were dark brown or black, fusiform, with regular margins (Fig. 1a). Subsequently, spots expanded and became light brown and water-soaked. Occasionally, several spots coalesced into a large lesion (Fig. 1b). When the pathogen invaded the vascular bundle tissues, development of the lesions was more rapid along the veins on the leaf sheaths (Fig. 1c). Afterwards, dark or long black stripes developed from the leaf sheaths to the leaves (Fig. 1d), and tissue maceration and dark-brown rot symptoms were observed (Fig. 1d). Subsequently, the infected tissues expanded in a centripetal direction, causing the upper part of the leaf sheaths to die on young plants (Fig. 1f). In this case, the leaf sheaths on a plant were easily fractured (Fig. 1f). Frequently, the death of entire leaf sheaths was observed in a clump (Fig. 1g).

3.2 Pathogen isolation

Five samples of diseased tissue from five different sites were collected. First, the tissue sap of the five samples was inoculated to exclude saprophytic microbes. After repeating inoculation, bacterial strains were isolated from fresh lesions. After purification, five strains were selected for pathogenicity tests.

3.3 Pathogenicity tests

Pathogenicity tests indicated that five strains (DY01, DY02, DY03, DY04, and DY05) from *Z. latifolia* all induced the formation of diseased lesions on the leaf sheaths of *Z. latifolia* 3 d after inoculation (Fig. 2a). Symptoms of the dark brown lesions were similar to those observed on plants in the field (Fig. 1), and no disease was found on control leaf sheaths. The lesions expanded up and down the veins of leaf sheaths, and gradually became dark brown 6 d (Fig. 2b) and 9 d (Fig. 2c) after inoculation. Disease symptoms did not develop during the same period on the control leaf sheaths (Fig. 2d).

3.4 Strain identification

Observation of colonies grown on LB agar plates showed that the characteristics of colonies of the five strains were the same. The colonies were yellow, round, and smooth, with regular and flat borders. Microscopic

Fig. 1 Symptoms of shoot rot of *Zizania latifolia* in fields. (a) Initial dark spots (arrows); (b) A coalesced dark brown lesion; (c) A dark grey streak; (d) Long black streak; (e) Symptoms of dark-brown rot; (f) A partially dead and fractured leaf sheath; (g) Entirely dead leaf sheaths on a few plants.

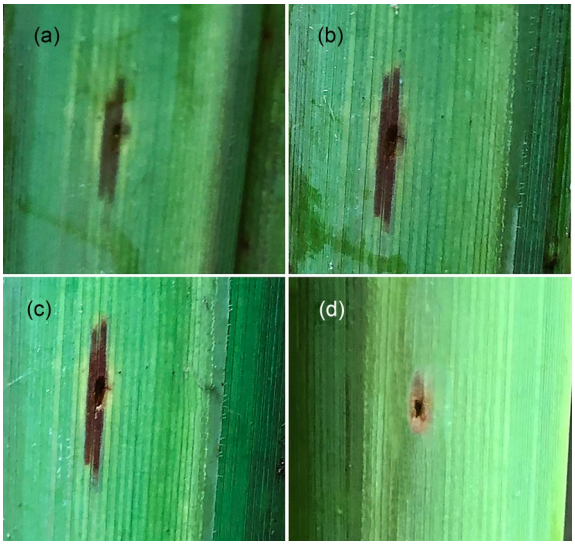

Fig. 2 Symptom variability on the leaf sheaths of *Zizania latifolia* after inoculation. (a) 3 d; (b) 6 d; (c) 9 d; (d) Control.

examination revealed that the strain was a Gram-negative bacillus with rounded ends. Analysis of 16S rRNA genes with the ClustalX (Version 1.83) showed that sequences of the five strains (DY01, DY02, DY03, DY04, and DY05) were identical. The results of the BLAST search showed that the five strains had an identity of 99.72%, with a variable score value of 2593 bits for *P. ananatis* (GenBank Nos. MG428916.1, MG428912.1, and MG428819.1). The sequences of the five strains were submitted to GenBank (Table S1). A phylogenetic tree was constructed using the 16S rRNA gene sequences to delineate the boundaries among closely related species in *Pantoea* (Fig. 3). This clearly showed that the five tested strains (DY01, DY02, DY03, DY04, and DY05) taken from the Jiaobai plants clustered with *P. ananatis* M27, LCFJ-001, and LMG2665 with high ML bootstrap (76%) support.

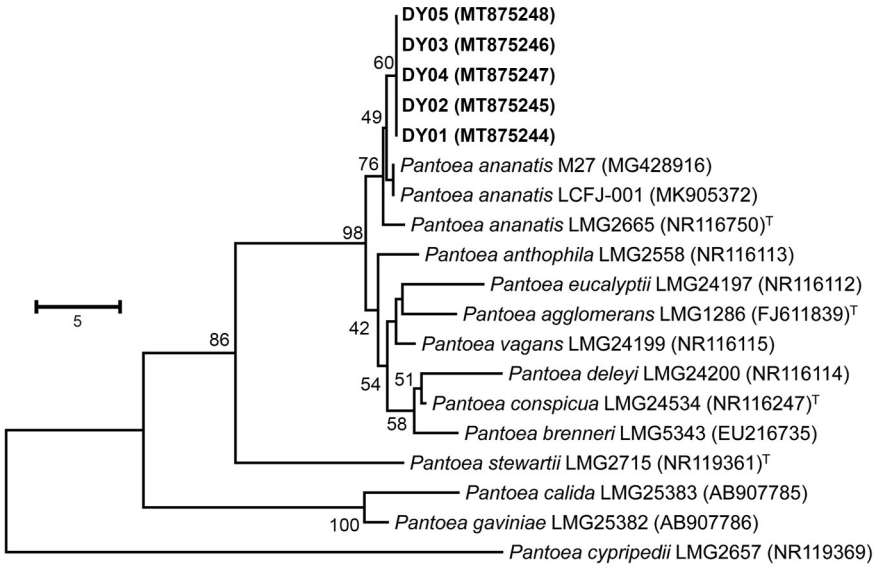

Fig. 3 Phylogenetic tree generated by the neighbor-joining method from 16S ribosomal RNA (rRNA) gene sequences of 19 taxa of *Pantoea*. Bootstrap values supporting the branches are shown at the nodes, and branch lengths are proportional to divergence. Strains isolated from the Jiaobai plants are shown in bold. T: type strain.

Furthermore, partial sequences of housekeeping genes, which are more reliable genetic markers for identification and phylogenetic analysis (Brady et al., 2008), were used in this study. A phylogenetic tree was constructed based on partial *gyrB*, *rpoB*, *infB*, and *atpD* sequences (Fig. 4). Phylogenetic analysis showed that the five tested strains taken from the Jiaobai plants clustered with the strains of *P. ananatis* (LMG2665^T, LMG2668, and LMG2676) as a distinct clade in the genus *Pantoea*, with high ML bootstrap (100%) support, forming a sister clade with *Pantoea allii* LMG24248 to the well-supported clade with high ML bootstrap (97%) support.

3.5 Observation of pathogen colonization

Ultrastructural observations demonstrated that the rod-shaped bacterial cells colonized vessels of *Z. latifolia* leaf sheaths and were scattered in the biofilm matrix of the inner wall surface of the vessels (Fig. 5a). The initial biofilms occurred on the concave inner wall surface of vessels (Fig. 5b), and were possibly involved in bacterial cell adhesion. The biofilm was composed of bacterial cells and a polymeric substance matrix (PSM) (Fig. 5c), as in other biofilm-growing bacteria (Tyson et al., 1985; Castiblanco and Sundin, 2016). Some bacterial cells embedded in the PSM had different sizes (Figs. 5d and 5e), and individual dividing cells could be observed (Fig. 5f), showing their different development stages. *P. ananatis* is a biofilm-forming bacterium that can grow and reproduce in invaded vessels, and biofilm formation is related to plant pathogenesis (Castiblanco and Sundin, 2016).

3.6 Primer specificity and reliability

Based on the complete genes being related to the classification of *Pantoea*, the *gyrB* sequence of *P. ananatis* had identities of 82.91%–87.31% with other species, showing the more significant base differences. The forward and reverse primers were designed after the *gyrB* sequences of different species were downloaded, aligned by BioEdit, analyzed, and assigned as pagyrB-F (5'-TACGGGAGATACCGATGC-3') and pagyrB-R (5'-GCGTGCGGCGTCAATAAT-3') (Fig. 6). The predicted products of PCR amplification had 673 base pairs (bp).

PCR amplification was conducted using the primer pairs pagyrB-F/R for the five strains of *P. ananatis* in this study, and the results showed that PCR products from the five strains could be observed (data not shown). The results of PCR amplification from 12 strains of *Pantoea* and other genera showed that the PCR product was observed only in *P. ananatis* DY01 and DY02 (Fig. 7a), confirming the specificity of the pagyrB-F/R. PCR amplification was used for the detection of *P. ananatis* in natural leaf sheaths. The

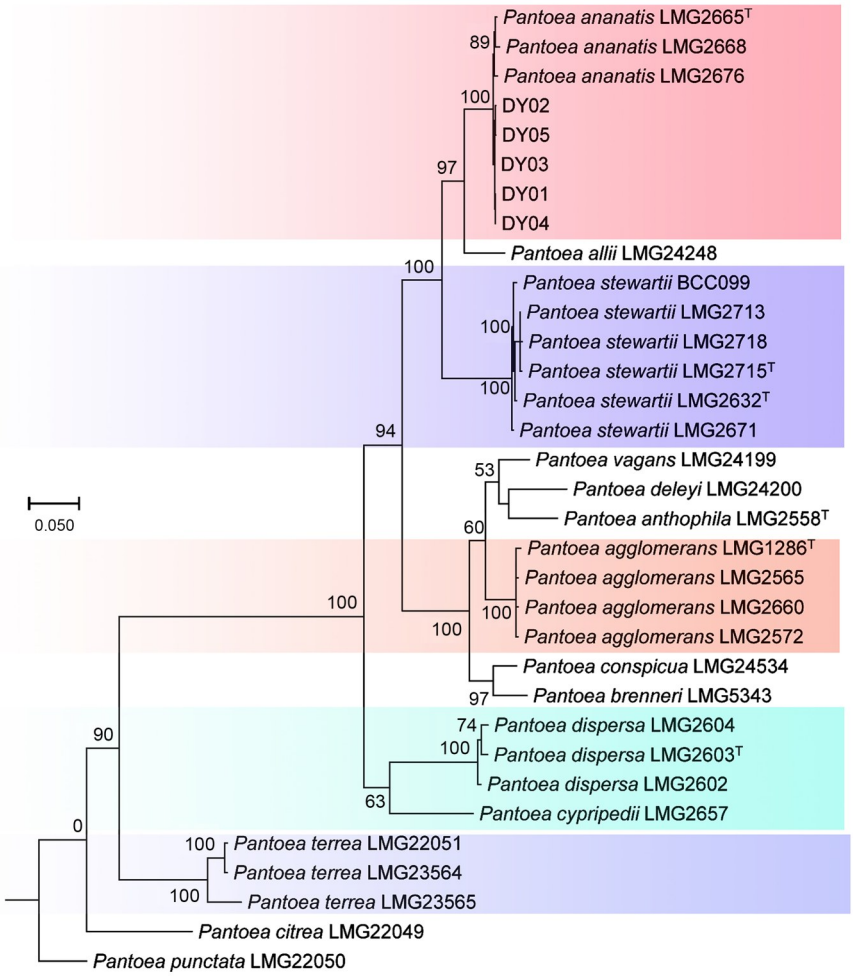

Fig. 4 Maximum-likelihood tree based on concatenated housekeeping gene (*atpD*, *gryB*, *infB*, and *rpoB*) sequences showing the relationships among members of strains of *Pantoea* spp. Bootstrap values (>50%) based on 1000 replicates are shown at branch nodes. *Pantoea punctate* LMG22050 was used as an outgroup. T: type strain.

results of PCR amplification showed that amplified products were observed from 12 samples of diseased leaf sheaths, but not from two samples of healthy leaf sheaths, confirming the reliability of the designed primers (Fig. 7b).

4 Discussion

P. ananatis strains are frequently found showing different mutualistic, saprophytic, and pathogenic associations with plants (Coutinho and Venter, 2009). Member of this species infect many mono- and dicotyledonous species, such as onion (Gitaitis and Gay, 1997), rice (Cother et al., 2004), maize (Paccola-Meirelles et al., 2001), sorghum (Cota et al., 2010), sudangrass (Azad et al., 2000), tomato (Stall et al., 1969), and melon (Wells et al., 1987). To our knowledge, this is the first record of shoot rot disease caused by *P. ananatis* on *Z. latifolia* in China.

Shoot rot of *Z. latifolia* shows typical leaf sheath stripes and rots, and symptoms of entire leaf sheath death, involved in the process of disease development. Although most initial spots or lesions were produced on the leaf sheaths, they sometimes appeared on a leaf near the sheath. Inward growth of lesions caused the enveloping leaf sheaths to rot and plants to die. The occurrence of the disease involves a source of inoculum and its dispersal. *P. ananatis* is an epiphyte that can exist on many plant or seed surfaces. These asymptomatic non-hosts can provide a source of inoculum, causing disease outbreaks in susceptible hosts grown in their vicinity (Coutinho and Venter, 2009). However, unlike seed-bearing plants, *Z. latifolia* can

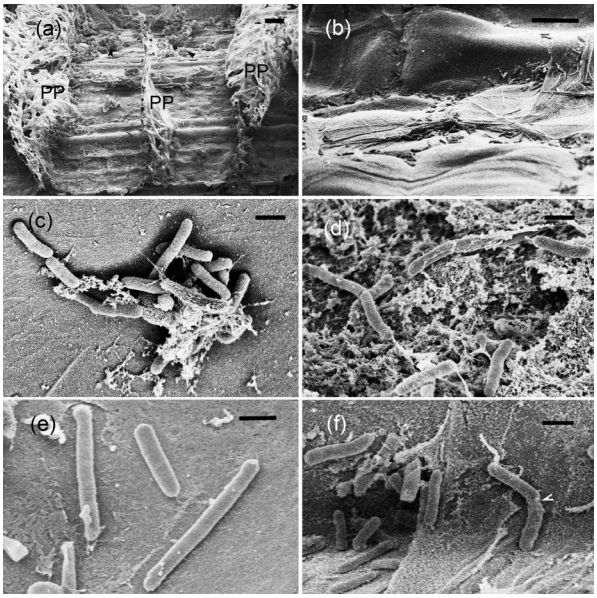

Fig. 5 Scanning electron micrographs of *Pantoea ananatis* DY03 colonizing a vessel of *Zizania latifolia*. (a) Biofilms (arrowheads) forming on the inner walls of the ruptured vessels. The biofilms did not occur on the perforated plates (PPs). Scale bar=50 μm. (b) Numerous bacterial cells at sites on the concave inner wall surface of a vessel. Scale bar=10 μm. (c) A biofilm with aggregated bacterial cells embedded in a polymeric substance matrix on a vessel wall. Scale bar=1 μm. (d) Bacterial cells of different sizes in a biofilm. Scale bar=1 μm. (e) Bacterial cells of different sizes. Scale bar=1 μm. (f) Individual dividing cell in a biofilm (arrowhead). Scale bar=1 μm.

be propagated from generation to generation using clonal propagules in aquatic ecosystems, and it is unclear how the pathogen survives and is dispersed. So further research should investigate the vector transmissibility, distribution, prevalence, and epidemiology of this pathogen.

The mechanisms of the diverse interactions between *P. ananatis* and the host are still poorly understood, although *P. ananatis* genomes and genomic differences in genes encoding protein secretion systems among different strains have been reported (de Maayer et al., 2014; Sheibani-Tezerji et al., 2015). In this study, pathogenicity assays were conducted on the leaf sheaths by inoculation with bacterial cell suspensions without media or with diseased tissue sap (data not shown). Lesion extension was more rapid following inoculation with bacterial cell suspensions without culture medium than following inoculation with diseased tissue sap 9 d after inoculation. Thus, nutrition increase may promote the growth and proliferation of this pathogen in plant tissues, causing larger lesions. The extension of lesions up and down the veins on the leaf sheaths (Figs. 2a–2c) might be related to bacterial cell colonization, dispersal, and pathogenic mechanisms.

Several plant pathogenic bacterial species, including *Erwinia amylovora*, *Pantoea stewartii*, *Ralstonia solanacearum*, *Xanthomonas campestris*, and *Xylella fastidiosa*, colonize or are hypothesized to colonize and form biofilms in xylem vessels (Castiblanco and Sundin, 2016). A few studies have shown that *P. stewartii* colonizes the xylem of the plant where it multiples and produces exo/capsular polysaccharide (EPS). EPS biosynthesis blocks the flow of water in a cell-density-dependent manner (Braun, 1982; Koutsoudis et al., 2006), causing the plant to wilt. However, there have been no reports of EPS production by *P. ananatis*. In this study, ultrastructural observations confirmed that the pathogen colonized in the vessels could grow and multiply (Figs. 5e and 5f). The studies revealed that bacterial cells passed easily through the

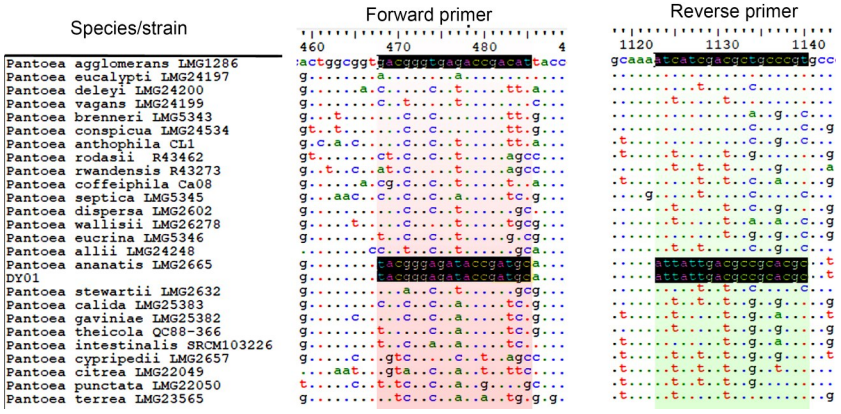

Fig. 6 Position of designed forward and reverse primers in the *gryB* gene in the genus *Pantoea* and their base differences among different species. Dark regions with two rows indicate the base sequences of the primers. Dots represent the same base.

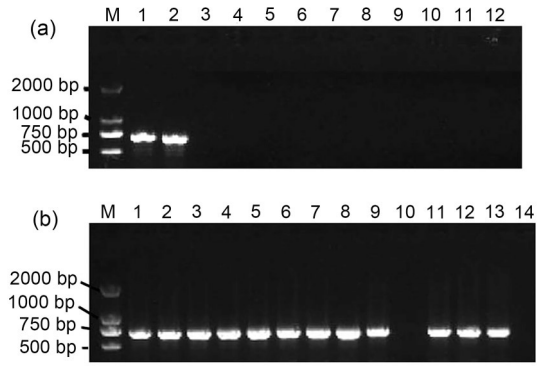

Fig. 7 Analysis of specificity and reliability of PCR amplification using the primer pairs pagyrB-F/R. (a) Electropherogram of the PCR-amplified DNA. Lanes 1–12: DNA templates from the isolates DY01 and DY02 of *Pantoea ananatis*, *Pantoea dispersa* LXQ1, *Pantoea allii* LXQ2, *Pantoea terrea* LXQ3, *Pantoea agglomerans* TY1, *Pseudomonas putida* IMA3, *Paenibacillus polymyxa* IMA5, *Bacillus cereus* IMA4, *B. cereus* IMA7, *Bacillus amyloliquefaciens* IMA1, and *B. amyloliquefaciens* IMA2, respectively. (b) Electropherogram of the PCR products. Lane 1: DNA template from the isolate DY01 of *P. ananatis*; Lanes 2–9 and 11–13: DNA templates from diseased samples of ZL01, ZL02, ZL03, ZL04, ZL05, ZL06, ZL07, ZL08, ZL10, ZL11, and ZL12, respectively; Lanes 10 and 14: DNA templates from healthy samples of ZL09 and ZL13, respectively. PCR: polymerase chain reaction; M: DNA marker.

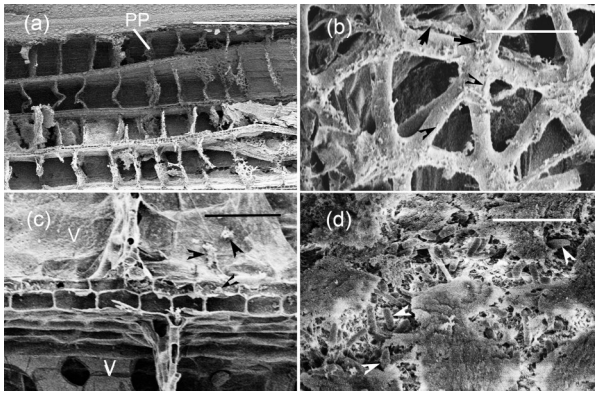

Fig. 8 Vessels with perforation plates (PPs) in a leaf sheath of *Zizania latifolia*. (a) Vessels with reticulate PP. Scale bar= 1000 μm. (b) A partial PP with triangular pores. Scale bar= 50 μm. Individual bacterial cells (arrowheads) and a few biofilms (arrows) are distributed on the reticulate ridges of a partial PP. (c) The biofilms (arrowheads) on the inner walls of a vessel (V) and tracheid cells. Scale bar=100 μm. (d) High magnification view of a biofilm (arrowheads) formation in a tracheid cell in (c). Scale bar=5 μm.

perforation plates (PPs) from one vessel element to the next in the vascular bundles of leaf sheaths, because the large reticulate pores on PPs were big enough to allow bacterial cells to pass through (Figs. 8a and 8b). Bacterial cells in the vessels could enter the adjacent tracheid cells (Fig. 8c), but not the PP blocked by the biofilms. The biofilm was composed of bacterial cells and host-derived materials (Fig. 8d), as reported by Braun (1982). Therefore, plant wilt may be related to the disintegration of vascular tissue. The disintegrated debris may block the flow of water, causing the plants to wilt or die. These are preliminary results, and further studies on the ultrastructural differences between susceptible and resistant hosts may provide crucial information on the virulence of *P. ananatis* among Jiaobai plant cultivars for crop management.

To prevent pathogen spread and disease occurrence, early detection of pathogens in seedlings is necessary. Molecular techniques based on PCR using species-specific primers have been extensively used to identify bacterial species. Several primer sets based on detecting the multiple copy 16S/23S regions have been used to detect *P. ananatis*, *P. stewartii*, and *P. allii* (Gitaitis et al., 2002; Carr et al., 2010; Figueiredo and Paccola-Meirelles, 2012). The primers PANA_1080 61F/1009R designed to detect *P. ananatis* from onion (Asselin et al., 2016) were used to detect *P. ananatis* in mixed cultures or environmental samples, but not in the diseased tissues of *Z. latifolia*. In this study, the primers reported herein have proven helpful for detecting the pathogen in the diseased tissues of *Z. latifolia*. Although the design and validation of primers for detecting the pathogenic bacterium should prove helpful for labs investigating bacterial shoot rot of *Z. latifolia*, the sensitivity of the primers for rapid detection of the pathogen before the disease occurs needs to be determined.

In brief, in this study, the pathogen causing shoot rot of Jiaobai was identified, the disease symptoms were described, ultrastructural characteristics of bacterial cell colonization and extension characteristics in diseased tissue were revealed, and a specific pair of primers was designed for detecting *P. ananatis*. This will provide important insights into disease pathogenesis and information for effective management of this disease in development of the Jiaobai industry.

5 Conclusions

A new disease, shoot rot of *Z. latifolia*, was found in Zhejiang Province, China. Symptoms of disease included lesions, streaks, sheath rot, and entire leaf

sheath death on young plants. The disease is caused by *P. ananatis*. This was confirmed by 16S rRNA gene sequencing, phylogenetic analysis using concatenated *atpD*, *gyrB*, *infB*, and *rpoB* gene sequences, and pathogenicity tests. Ultrastructural observations revealed that the pathogen colonized mainly the vascular tissues in leaf sheaths, forming biofilms, and extended within and between the vessels. The pathogen was detected by a specific pair of primers (pagyrB-F/R) designed and validated by PCR amplification of DNA of closely related and unrelated species and the diseased tissues of *Z. latifolia*. To our knowledge, this is the first report of bacterial sheath rot disease of *Z. latifolia* caused by *P. ananatis* in China.

Acknowledgments

This work was supported by the Key Project of National Natural Science Foundation of China (NSFC) Regional Innovation and Development Joint Foundation (No. U20A2043) and the NSFC (No. 31501342).

Author contributions

Zilan XIAO performed the experimental research and data analysis, and wrote the manuscript. Jianping DENG, Xiaojun ZHOU, Liyan ZHU, and Xiaochan HE provided the samples. Jingwu ZHENG and Deping GUO performed the data analysis. Jingze ZHANG contributed to the study design, writing and editing of the manuscript. All authors have read and approved the final manuscript, and therefore, have full access to all the data in the study and take responsibility for the integrity and security of the data.

Compliance with ethics guidelines

Zilan XIAO, Jianping DENG, Xiaojun ZHOU, Liyan ZHU, Xiaochan HE, Jingwu ZHENG, Deping GUO, and Jingze ZHANG declare that they have no conflict of interest.

This article does not contain any studies with human or animal subjects performed by any of the authors.

References

Ann PJ, Huang JH, Wang IT, et al., 2006. *Pythiogeton zizaniae*, a new species causing basal stalk rot of water bamboo in Taiwan. *Mycologia*, 98(1):116-120. https://doi.org/10.1080/15572536.2006.11832717

Asselin JAE, Bonasera JM, Beer SV, 2016. PCR primers for detection of *Pantoea ananatis*, *Burkholderia* spp. and *Enterobacter* sp. from onion. *Plant Dis*, 100(4):836-846. https://doi.org/10.1094/PDIS-08-15-0941-RE

Azad HR, Holmes GJ, Cooksey DA, 2000. A new leaf blotch disease of sudangrass caused by *Pantoea ananas* and *Pantoea stewartii*. *Plant Dis*, 84(9):973-979. https://doi.org/10.1094/PDIS.2000.84.9.973

Brady C, Cleenwerck I, Venter S, et al., 2008. Phylogeny and identification of *Pantoea* species associated with plants, humans and the natural environment based on multilocus sequence analysis (MLSA). *Syst Appl Microbiol*, 31(6-8): 447-460. https://doi.org/10.1016/j.syapm.2008.09.004

Braun EJ, 1982. Ultrastructural investigation of resistant and susceptible maize inbreds infected with *Erwinia Stewartii*. *Phytopathology*, 72(1):159-166. https://doi.org/10.1094/Phyto-77-159

Carr EA, Bonasera JM, Zaid AM, et al., 2010. First report of bulb disease of onion caused by *Pantoea ananatis* in New York. *Plant Dis*, 94(7):916. https://doi.org/10.1094/PDIS-94-7-0916B

Castiblanco LF, Sundin GW, 2016. New insights on molecular regulation of biofilm formation in plant-associated bacteria. *J Integr Plant Biol*, 58(4):362-372. https://doi.org/10.1111/jipb.12428

Cota LV, Costa RV, Silva DD, et al., 2010. First report of pathogenicity of *Pantoea ananatis* in sorghum (*Sorghum bicolor*) in Brazil. *Austral Plant Dis Notes*, 5(1):120-122. https://doi.org/10.1071/DN10044

Cother EJ, Reinke R, McKenzie C, et al., 2004. An unusual stem necrosis of rice caused by *Pantoea ananas* and the first record of this pathogen on rice in Australia. *Austral Plant Pathol*, 33(4):495-503. https://doi.org/10.1071/AP04053

Coutinho TA, Venter SN, 2009. *Pantoea ananatis*: an unconventional plant pathogen. *Mol Plant Pathol*, 10(3):325-335. https://doi.org/10.1111/j.1364-3703.2009.00542.x

Darriba D, Taboada GL, Doallo R, et al., 2012. jModelTest 2: more models, new heuristics and parallel computing. *Nat Methods*, 9(8):772. https://doi.org/10.1038/nmeth.2109

de Maayer P, Chan WY, Rubagotti E, et al., 2014. Analysis of the *Pantoea ananatis* pan-genome reveals factors underlying its ability to colonize and interact with plant, insect and vertebrate hosts. *BMC Genomics*, 15:404. https://doi.org/10.1186/1471-2164-15-404

Deng JP, Zhang JZ, Hu MH, 2015. Occurrence regularity and control of Jiaobai rust in Dayang Town, Jinyun County. *J Chang Jiang Veget*, (17):51-53 (in Chinese). https://doi.org/10.3865/j.issn.1001-3547.2015.17.025

Figueiredo JEF, Paccola-Meirelles LD, 2012. Simple, rapid and accurate PCR-based detection of *Pantoea ananatis* in maize, sorghum and *Digitaria* sp. *J Plant Pathol*, 94(3): 663-667. https://doi.org/10.4454/JPP.FA.2012.049

Gitaitis R, Walcott R, Culpepper S, et al., 2002. Recovery of *Pantoea ananatis*, causal agent of center rot of onion, from weeds and crops in Georgia, USA. *Crop Prot*, 21(10): 983-989. https://doi.org/10.1016/S0261-2194(02)00078-9

Gitaitis RD, Gay JD, 1997. First report of a leaf blight, seed stalk rot, and bulb decay of onion by *Pantoea ananas* in Georgia. *Plant Dis*, 81(9):1096. https://doi.org/10.1094/PDIS.1997.81.9.1096C

Hall TA, 1999. Bioedit: a user-friendly biological sequence

alignment editor and analysis program for Windows 95/98/NT. *Nucl Acids Symp Ser*, 41:95-98.

Katoh K, Standley DM, 2013. MAFFT multiple sequence alignment software Version 7: improvements in performance and usability. *Mol Biol Evol*, 30(4):772-780. https://doi.org/10.1093/molbev/mst010

Koutsoudis MD, Tsaltas D, Minogue TD, et al., 2006. Quorum-sensing regulation governs bacterial adhesion, biofilm development, and host colonization in *Pantoea stewartii* subspecies *stewartii*. *Proc Natl Acad Sci USA*, 103(15):5983-5988. https://doi.org/10.1073/pnas.0509860103

Kumar S, Stecher G, Tamura K, 2016. MEGA7: Molecular Evolutionary Genetics Analysis Version 7.0 for bigger datasets. *Mol Biol Evol*, 33(7):1870-1874. https://doi.org/10.1093/molbev/msw054

Lane DJ, 1991. 16S/23S rRNA sequencing. *In*: Stackebrandt E, Goodfellow M (Eds.), Nucleic Acid Techniques in Bacterial Systematics. Wiley, Chichester, p.115-175.

Lane DJ, Pace B, Olsen GJ, et al., 1985. Rapid determination of 16S ribosomal RNA sequences for phylogenetic analyses. *Proc Natl Acad Sci USA*, 82(20):6955-6959. https://doi.org/10.1073/pnas.82.20.6955

Li XL, Ojaghian MR, Zhang JZ, et al., 2017. A new species of *Scopulariopsis* and its synergistic effect on pathogenicity of *Verticillium dahliae* on cotton plants. *Microbiol Res*, 201:12-20. https://doi.org/10.1016/j.micres.2017.04.006

Nisikado Y, 1929. Studies on the *Helminthosporium* diseases of *Gramineae* in Japan. *Ber Ohara Inst Landw Forsch*, 4(1):111-126.

Paccola-Meirelles LD, Ferreira AS, Meirelles WF, et al., 2001. Detection of a bacterium associated with a leaf spot disease of maize in Brazil. *J Phytopathol*, 149(5):275-279. https://doi.org/10.1046/j.1439-0434.2001.00614.x

Sheibani-Tezerji R, Naveed M, Jehl MA, et al., 2015. The genomes of closely related *Pantoea ananatis* maize seed endophytes having different effects on the host plant differ in secretion system genes and mobile genetic elements. *Front Microbiol*, 6:440. https://doi.org/10.3389/fmicb.2015.00440

Shoemaker RA, 2006. Nomenclature of *Drechslera* and *Bipolaris*, grass parasites segregated from '*Helminthosporium*'. *Can J Plant Pathol*, 28(S1):S212-S220. https://doi.org/10.1080/07060660609507377

Silvestro D, Michalak I, 2012. raxmlGUI: a graphical front-end for RAxML. *Org Divers Evol*, 12(4):335-337. https://doi.org/10.1007/s13127-011-0056-0

Stall RE, Alexander LJ, Hall CB, 1969. Effect of tobacco mosaic virus and bacterial infections on occurrence of graywall of tomato. *Proc Fla State Hortic Soc*, 82:157-161.

Talavera G, Castresana J, 2007. Improvement of phylogenies after removing divergent and ambiguously aligned blocks from protein sequence alignments. *Syst Biol*, 56(4):564-577. https://doi.org/10.1080/10635150701472164

Turner S, Pryer KM, Miao VPW, et al , 1999. Investigating deep phylogenetic relationships among cyanobacteria and plastids by small subunit rRNA sequence analysis. *J Eukaryot Microbiol*, 46(4):327-338. https://doi.org/10.1111/j.1550-7408.1999.tb04612.x

Tyson GE, Stojanovic BJ, Kuklinski RF, et al., 1985. Scanning electron microscopy of Pierce's disease bacterium in petiolar xylem of grape leaves. *Phytopathology*, 75(3):264-269.

Vaidya G, Lohman DJ, Meier R, 2011. SequenceMatrix: concatenation software for the fast assembly of multi-gene datasets with character set and codon information. *Cladistics*, 27(2):171-180. https://doi.org/10.1111/j.1096-0031.2010.00329.x

Wells JM, Sheng WS, Ceponis MJ, et al., 1987. Isolation and characterization of strains of *Erwinia ananas* from honeydew melons. *Phytopathology*, 77(3):511-514.

Xiao ZL, Hyde KD, Zhang JZ, 2015. Synonymy of two species of *Bipolaris* from aquatic crops of *Poaceae*. *Mycotaxon*, 130(1):131-143. https://doi.org/10.5248/130.131

Xu XW, Walters C, Antolin MF, et al., 2009. Phylogeny and biogeography of the eastern Asian-North American disjunct wild-rice genus (*Zizania* L., Poaceae). *Mol Phylogenet Evol*, 55(3):1008-1017. https://doi.org/10.1016/j.ympev.2009.11.018

Zhang F, Li XL, Zhu SJ, et al., 2018. Biocontrol potential of *Paenibacillus polymyxa* against *Verticillium dahliae* infecting cotton plants. *Biol Control*, 127:70-77. https://doi.org/10.1016/j.biocontrol.2018.08.021

Zhang JZ, Chu FQ, Guo DP, et al., 2012. Cytology and ultrastructure of interactions between *Ustilago esculenta* and *Zizania latifolia*. *Mycol Prog*, 11(2):499-508. https://doi.org/10.1007/s11557-011-0765-y

Zhang JZ, Chu FQ, Guo DP, et al., 2014. The vacuoles containing multivesicular bodies: a new observation in interaction between *Ustilago esculenta* and *Zizania latifolia*. *Eur J Plant Pathol*, 138(1):79-91. https://doi.org/10.1007/s10658-013-0303-7

Supplementary information

Table S1